Spin to Charge Conversion at Room Temperature by Spin Pumping into a New Type of Topological Insulator: α-Sn Films

J.-C. Rojas-Sánchez,[1,*] S. Oyarzún,[2,3] Y. Fu,[2,3] A. Marty,[2,3] C. Vergnaud,[2,3] S. Gambarelli,[2,3] L. Vila,[2,3] M. Jamet,[2,3] Y. Ohtsubo,[4,5] A. Taleb-Ibrahimi,[6,7] P. Le Fèvre,[7] F. Bertran,[7] N. Reyren,[1,†] J.-M. George,[1] and A. Fert[1,‡]

[1]*Unité Mixte de Physique, CNRS, Thales, Univ. Paris-Sud, Université Paris-Saclay, 91767 Palaiseau, France*

[2]*Université Grenoble Alpes, INAC-SP2M, F-38000 Grenoble, France*

[3]*CEA, Institut Nanosciences et Cryogénie, F-38000 Grenoble, France*

[4]*Graduate School of Frontier Biosciences, Osaka University, Suita 565-0871, Japan*

[5]*Graduate School of Science, Osaka University, Toyonaka 560-0043, Japan*

[6]*UR1 CNRS, Synchrotron SOLEIL, Saint-Aubin, 91192 Gif sur Yvette, France*

[7]*Synchrotron SOLEIL, Saint-Aubin, 91192 Gif sur Yvette, France*

(Received 18 December 2015; published 1 March 2016)

We present results on spin to charge current conversion in experiments of resonant spin pumping into the Dirac cone with helical spin polarization of the elemental topological insulator (TI) α-Sn. By angle-resolved photoelectron spectroscopy (ARPES), we first check that the Dirac cone (DC) at the α-Sn (0 0 1) surface subsists after covering Sn with Ag. Then we show that resonant spin pumping at room temperature from Fe through Ag into α-Sn layers induces a lateral charge current that can be ascribed to the inverse Edelstein effect by the DC states. Our observation of an inverse Edelstein effect length much longer than those generally found for Rashba interfaces demonstrates the potential of TIs for the conversion between spin and charge in spintronic devices. By comparing our results with data on the relaxation time of TI free surface states from time-resolved ARPES, we can anticipate the ultimate potential of the TI for spin to charge conversion and the conditions to reach it.

DOI: 10.1103/PhysRevLett.116.096602

Most spintronics devices [1] are today based on the manipulation of spin currents that do not carry electrical charges but can be described as equal flows of electrons with opposite spins in opposite directions. The main operations in spintronics are the creation of spin currents from charge currents (electrical currents) and the detection of spin currents by transforming them into charge currents, in other words, conversions between charge and spin currents. Classical spintronics generally uses magnetic materials for these conversions, but it now appears that they can also be obtained by harnessing the spin-orbit coupling (SOC), the relativistic correction to the equation of quantum physics that can be significantly strong in materials containing heavy atoms. Typical examples of SOC effects are the spin Hall effect (SHE) of heavy metals by which a charge current can be converted into a transverse spin current and the inverse spin Hall effect (ISHE) for the inverse conversion [2]. An example of an application based on SHE is the so-called spin-orbit torque random access memory [3]. Today, it turns out that a more efficient conversion can be obtained by exploiting the SOC-induced properties of a two-dimensional electron gas (2DEG) at some surfaces and interfaces, the so-called Rashba interfaces [4] and the surfaces or interfaces of new materials called topological insulators (TIs) [5–9].

The electronic states of the 2DEG at Rashba interfaces (for example, Bi|Ag [4]) or at the surfaces or interfaces of a TI [5–9] are characterized by a locking between spin and momentum by SOC. Figures 1(a) and 1(b) present an artist's view of dispersion surfaces of Rashba states (a) and Dirac dispersion cones (DCs) at a TI surface or interface (b), as well as the helical spin configuration associated with the spin-momentum locking on their respective Fermi contours. Dirac cones and Fermi contours similar to those in Fig. 1(b) have been characterized in the recently discovered TI α-Sn [10,11]. As depicted in Figs. 1(c) and 1(d), a current carried by a 2DEG with helical spin polarization is automatically accompanied by a nonzero spin accumulation with the spins along the in-plane direction transverse to the current. This effect has been predicted in 1990 by Edelstein [12] and can be described as a charge to spin conversion effect [13]. The Edelstein effect (EE) has been recently demonstrated by spin-polarized positron experiments [14] for the Rashba interface Bi|Ag and has been also observed in experiments with TIs [15–17].

The inverse Edelstein effect (IEE) [18–23] can be described as the inverse conversion of the one in the EE. As depicted in Figs. 1(e) and 1(f), the injection of a vertical spin current into 2DEGs at a Rashba or TI surface or interface induces a charge current in the 2DEG. The IEE length λ_{IEE} [18–23] is the ratio between the 2D horizontal charge current density j_C^{2D} (in A/m) induced by IEE in the surface or interface 2DEG and the injected vertical 3D spin

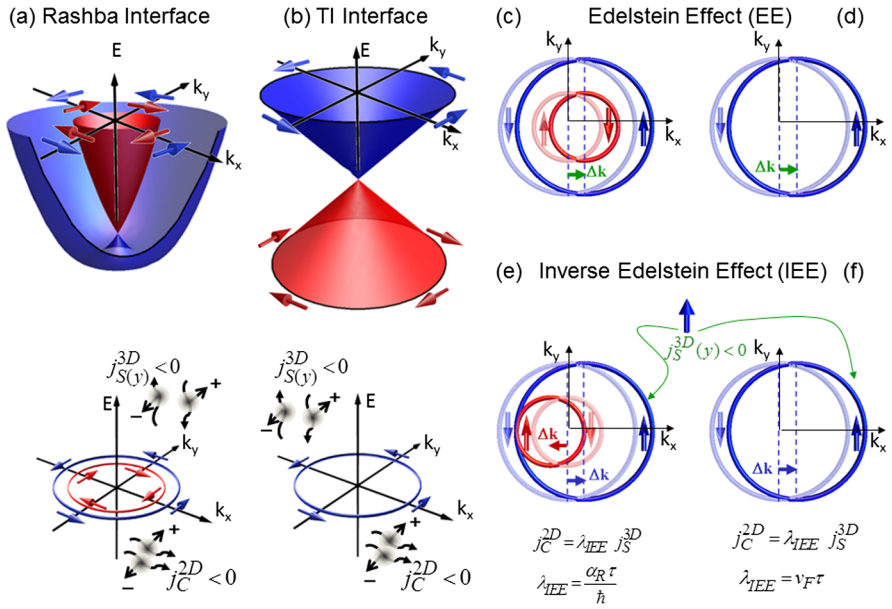

FIG. 1. Edelstein and inverse Edelstein effect. (a),(b) Top: Energy dispersion surfaces of the 2D states at a Rashba interface (a) and Dirac dispersion cone of the surface or interface states of a topological insulator (b). Bottom: Fermi contours of Rashba states (a) with two contours with helical spin configurations of opposite chirality and TI surface or interface states (b). (c),(d) Edelstein effect: A flow of electrons along x ($j_C{}^{2D(x)} < 0$ in the figure) in Rashba (c) or TI (d) 2DEGs is associated with shifts Δk of the Fermi contours generating an extra population of spin along the y direction (for Rashba there is a partial compensation of the contributions of the two contours). (e), (f) Inverse Edelstein effect: Injection of a spin current density spin polarized along y ($j_{S(y)}{}^{3D} < 0$ in the figure) into Rashba (e) or TI (f) 2DEGs induces an extra population on one of the sides of the Fermi contour (along the x direction), a depletion on the other side, and therefore a charge current density $j_C{}^{2D(x)}$ (<0 in the figure). $j_{S(y)}{}^{3D}$ and $j_C{}^{2D(x)}$ of this figure can be seen as carried by the electrons of the wave vector (wavy arrow) and spin (straight arrow) in the schematic at the bottom of (a) and (b). For a circular Fermi contour, the expressions of the IEE length λ_{IEE} are given in the bottom right of the figure as a function of the relaxation time of the topological states and Rashba coefficient α_R or Fermi velocity v_F of the DC. All the figures are drawn for electron-type conduction in the 2D states.

current density $j^{3\mathrm{D}}_{S(i)}$. Note that we define the spin current density $j^{3\mathrm{D}}_{S(i)}$ as the difference between the charge current densities along z carried by electrons having their spin along $\pm i$ ($i = x$ or y), so that the corresponding injected spin flow density is $j^{3\mathrm{D}}_{S(i)}\hbar/2e$, where $e = -|e|$. For both Rashba and TI interfaces, and in the simple situation of circular spin contours, λ_{IEE} can be expressed as a function of the relaxation time τ of an out-of-equilibrium distribution in the topological states by the expressions: $\lambda_{\mathrm{IEE}} = \alpha_R\tau/\hbar$ for Rashba interfaces [18,19], where α_R is the Rashba coefficient, and

$$\lambda_{\mathrm{IEE}} = v_F\tau, \tag{1}$$

where v_F is the Fermi velocity of the DC for the TI [24]. λ_{IEE} is defined as $j_C^{2\mathrm{D}(x)}/j^{3\mathrm{D}}_{S(y)}$ or $-j_C^{2\mathrm{D}(y)}/j^{3\mathrm{D}}_{S(x)}$, where the upper (lower) index refers to the positive current (spin quantization) axes. With this choice of definition, for the same spin injection, a positive λ_{IEE} produces a current in the same direction as an ISHE with a positive spin Hall angle (example: Pt). λ_{IEE} is expected to be positive for the situation of spin injection into a counterclockwise (CCW) helical Fermi contour of electrons [Figs. 1(a) and 1(b) and Ref. [24]].

The spin to charge conversion by IEE was first demonstrated by resonant spin pumping onto Bi|Ag Rashba interfaces [18], and this approach was then extended to other Rashba interfaces [20–23] and to TIs [24,27,28]. The spin-charge current conversion (SCC) has also been obtained by tunneling spin injection into TIs [29]. Here we present spin pumping experiments on thin α-Sn (0 0 1) films, a recently characterized new type of TI [9–11]. They reveal an unprecedented SCC efficiency by IEE. The SCC by EE and IEE is promising for the generation and detection of spin currents in spintronic devices, but for applications, an efficient conversion subsisting at room temperature (RT), as we find with α-Sn, is also mandatory.

Band gap opening and TI properties can be induced in α-Sn (0 0 1) layers either by strain or quantum-size effects in thin films [9–11]. Recent ARPES measurements of Ohtsubo *et al.* [11] performed on thin α-Sn (0 0 1) films grown *in situ* by molecular beam epitaxy have revealed a Dirac cone (DC) linear dispersion with helical spin polarization around the Γ point of the surface Brillouin zone for thicknesses between about 24 and 34 monolayers (ML). The Fermi energy E_F is in the lower cone at 20 meV below the Dirac point for 24 ML and in the upper cone for 30–34 ML. The spin-resolved ARPES indicated clockwise

(CW) or CCW spin helicity in the lower or upper cone, respectively.

For our experiments, as described in Ref. [24], InSb(001)|α-Sn(001), InSb(001)|α-Sn(001)|Fe, and InSb(001)|α-Sn(001)|Ag|Fe samples with 30 ML thick α-Sn(001) layers were grown by molecular beam epitaxy inside the Cassiopee beam line of the synchrotron SOLEIL in the same conditions and in the same beam line as those used by Ohtsubo *et al.*[11] (details in [24]). The growth inside the beam line allows us to check by ARPES (Fig. 2) if the DC subsists after covering α-Sn by thin Fe or Ag layers and before growing the complete structure of Fig. 3(a) and taking it off for spin pumping.

In the ARPES images of Fig. 2, a DC is clearly seen at the free surface (top surface) of α-Sn(001), and it disappears for Fe coatings as thin as half of a monolayer, i.e., 0.09 nm (left), but subsists when α-Sn is covered with even 1.2 nm of Ag (right). As shown in Ref. [24], we find that, without and with Ag, the Fermi energy E_F is in the upper cone as in the results of Ohtsubo *et al.* [11] for 30 ML, and its distance from the energy of the Dirac point (E_{DP}) is larger ($\sim 75 \pm 8$ meV) with Ag [24] than for the free surface of α-Sn ($\sim$30 meV). The slopes of the DC do not depend significantly on the direction in k space (compare [100] and [110] on the top images in Fig. 2), which justifies a picture with an approximately circular Fermi contour and the use of Eq. (1), and they correspond to a Fermi velocity v_F around 6.0×10^5 m/s without Ag and 5.6×10^5 m/s with Ag [24]. As the DC does not subsist with Fe, we can thus expect that only the α-Sn|Ag|Fe samples will show SCC by IEE (and not the α-Sn|Fe ones).

The correlation between the existence of a DC at the surface of α-Sn covered by Ag and the observation of SCC, as well as the absence of SCC with Fe directly on α-Sn, is confirmed by the results in Figs. 3(b) and 3(c). The main points are as follows: (i) A large enhancement of the

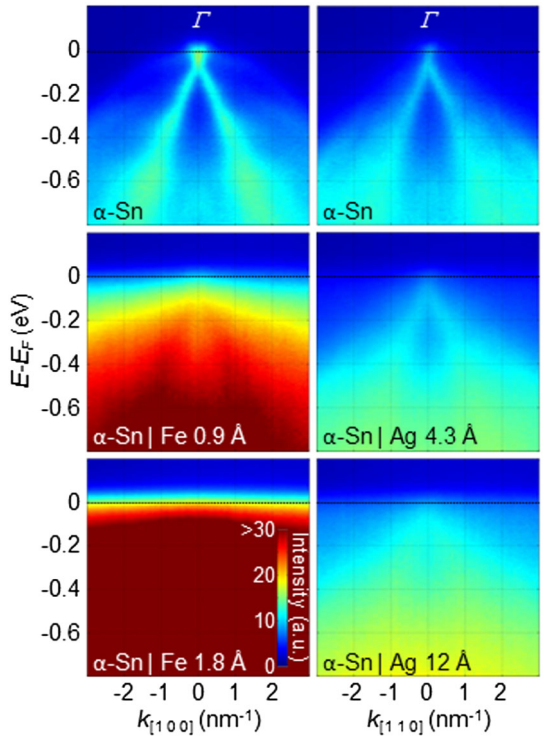

FIG. 2. ARPES characterization of the interfaces states of α-Sn (0 0 1) films covered by Fe or Ag. Top: ARPES intensity plots of the DC along [100] or [110] on the free surface of α-Sn (approximately 30 ML thick). Below: ARPES plots after covering by 0.9 or 1.8 Å of Fe (left) and 4.3 or 12 Å of Ag (right). The intensity is color coded with the same color scale in each panel (arbitrary units).The DC subsists if α-Sn is covered by Ag, and it can still be seen when the Sn|Ag interface is buried below 12 Å of Ag. It disappears after covering by Fe, but the overlap with the high intensity of the Fe 3d band dispersion at the Fermi level precludes definitive conclusions on the complete suppression of the DC.

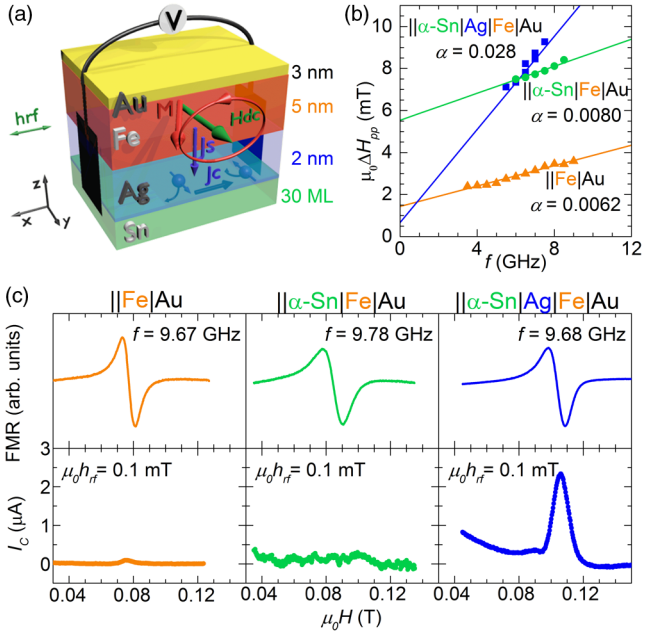

FIG. 3. Spin to charge current conversion by spin pumping into the topological states of α-Sn (0 0 1). (a) Experimental setup for spin pumping into α-Sn by ferromagnetic resonance (FMR) of a Fe layer [24]. (b) Broadband frequency dependence of the peak-to-peak FMR linewidth when the magnetic field H is applied along the [1 0 0] direction of the InSb substrate for InSb|Fe|Au (reference for the Fe layer), InSb|α-Sn|Fe|Au, and InSb|α-Sn|Ag|Fe|Au samples. The effective damping coefficient of Fe, proportional to the slopes, is definitely larger with the Ag interface ($\alpha = 0.028$ compared to 0.008 and 0.006 for the two other structures), which shows the strong spin absorption by the α-Sn|Ag interface. (c) FMR and dc charge current signals from measurements in a cylindrical X-band resonant cavity on InSb|Fe|Au, InSb|α-Sn|Fe|Au, and InSb|α-Sn|Ag|Fe|Au samples. Only the third sample shows a dc current signal in agreement with the observation of a Dirac cone at only the α-Sn|Ag interface.

damping coefficient revealing significant spin absorption is seen in Fig. 3(b) only for α-Sn|Ag|Fe and not for α-Sn|Fe. (ii) In Fig. 3(c), a dc charge current I_c peak at the resonance is only seen for α-Sn|Ag|Fe (left figure). As the direct contact of Fe on α-Sn suppresses the Dirac cone of the surface states but should not change the spin injection into the lower part of the film, the absence of a charge current signal for the α-Sn|Fe samples [central part of Fig. 3(c)] shows that the SCC seen for α-Sn|Ag|Fe comes only from the interface (a contribution from the spin Hall effect of the Ag layer can also be ruled out as shown by previous experiments with Ag layers in the same thickness range [18]).

We used the standard analysis of spin pumping on SHE materials [30,31], a Rashba system [18,20–22] and TIs [27,28,32] to extract [24] the injected vertical spin current density j_S^{3D}, the resulting 2D lateral charge current density $j_C^{2D} = I_C/(\text{width})$, and finally, using $\lambda_{IEE} = j_C^{2D}/j_S^{3D}$ as defined just after Eq. (1), the IEE length $\lambda_{IEE} = 2.1$ nm characterizing the SCC by the Dirac states at the Sn/Ag interface (we have shown a few lines above why additional contributions from below or above this interface can be excluded). The positive sign of λ_{IEE} is consistent [24] with the CCW helical spin configuration of the electron-type Fermi contours in α-Sn [11].

The parameter characterizing the spin to charge conversion by our α-Sn|Ag|Fe samples, $\lambda_{IEE} = 2.1$ nm, is one order of magnitude larger than $\lambda_{IEE} \approx 0.1$–$0.4$ nm found at the Bi|Ag and various other Rashba interfaces [18,20–23], as it could be expected from the disadvantage of the partial compensation of the two Fermi contours of Rashba 2DEGs.

Shiomi *et al.* [27] also observed SCC by spin pumping on several TI but only at a low temperature and explained the weak efficiency of the conversion by a reduction factor $\eta = 10^{-4}$ ascribed to "the imperfect insulation of the bulk states." By spin pumping on Bi_2Se_3, Deorani *et al.* [28] found that the SCC signal includes contributions from both the bulk part of the sample and the "surface layer" supposed to be 3 nm thick with an ISHE characterized by its spin Hall angle (SHA) θ_{SHE} (ratio between spin and charge 3D current densities) and a spin coherence length l_{sf}. Actually, the SCC by ISHE in such a surface layer can be expressed in terms of an IEE length if one integrates the ISHE-induced 3D charge current density from top to bottom of the surface layer to obtain the 2D charge current density. The maximum value of the 2D charge current for $t \gg l_{sf}$ is $j_C^{2D}(\text{ISHE}) = \Theta_{SHE} l_{sf} j_S^{3D}$ and corresponds to a maximum possible value of the IEE length equal to $\lambda^* = \theta_{SHE} l_{sf}$ [24], so that the results of Deorani *et al.* [28], $\theta_{SHE} \sim 0.01$ and $l_{sf} \sim 6$ nm at RT for the surface layer, correspond to a maximum value of IREE length equal to about 6×10^{-2} nm, well below $\lambda_{IEE} = 2$ nm with α-Sn. Jamali *et al.* [32] also observed SCC with Bi_2Se_3 but did not separate the bulk and surface contributions.

It also turns out that the SCC by α-Sn is definitely better, in terms of efficiency, than what can be obtained by the 3D SHE or 3D ISHE of the Pt or W layers used in most applications. We again consider that, in the optimal situation with layers thicker than a few l_{sf}, the maximum 2D charge current induced by ISHE is equivalent to the 2D current production by an effective IEE length $\lambda^* = \theta_{SHE} l_{sf}$ [24]. For Pt, with $l_{sf} \approx 3.4$ nm and $\theta_{SHE} \approx 0.056$ [31], the conversion efficiency of α-Sn, $\lambda_{IEE} = 2.1$ nm, could be obtained with a SHA equal to 0.62, a value 10 times larger than the SHA of Pt, $\theta_{SHE} \approx 0.05$ [31]. For thin W films, with $l_{sf} \approx 1.3$ nm [33], the conversion efficiency of α-Sn would be obtained with a SHA as large as 1.6, well above the SHA of W in the literature, $\theta_{SHE} \approx 0.33$ [34] or 0.27 [33].

In the situation of an approximately circular Fermi contour justified by our ARPES data (see also [24]), Eq. (1) can be used to derive the relaxation time τ of out-of-equilibrium distributions in the topological states from the IEE length λ_{IEE} and the Fermi velocity v_F. Using $\lambda_{IEE} \approx 2.1$ nm and $v_F \approx 5.6 \times 10^5$ m/s, we find $\tau \approx 3.7$ fs. Interestingly, the τ derived from spin pumping on TI or Rashba "interfaces" (5 fs for the Bi|Ag Rashba interface [18]) are definitely shorter than the relaxation times in the picosecond range derived from time-resolved ARPES measurements on "free surfaces" of TI [35]. We suggest that the long relaxation time on free topological surfaces characterizes the slow relaxation inside the DC, whereas, by interfacing the TI with a metal such as Ag, we introduce a faster additional relaxation mechanism provided by spin-flips in the exchange of electrons with the adjacent metal. We conclude that the best conditions for the exploitation of topological states of TIs in spintronics should be with TIs interfaced with insulators instead of metals, for example, in experiments of spin pumping or thermal [36] spin injection from an insulating ferromagnet. If one remarks that $v_F\tau$ is also the critical length for ballistic transport, one can also anticipate that ballistic transport should be generally limited to the nanometer range at a TI-metal interface but can probably reach or exceed the micrometer range on free surfaces and possibly at interfaces with insulating materials.

In summary, a very efficient spin to charge SCC at room temperature is achieved by spin pumping into the recently discovered topological insulator α-Sn in thin films, in clear relation with the IEE induced by the CCW helical spin configuration of the Dirac cones that we have identified by ARPES at the α-Sn(001)|Ag interface. To our knowledge, these results are the first combining ARPES characterization of Dirac cones and SCC by IEE on the same series of samples. We have also used a parameterization of the SCC recently introduced for Rashba interface states [18,20–22] but, to our knowledge, never for TI interfaces. The efficient SCC at RT by α-Sn films is certainly promising for spintronic devices. On the other hand, the theoretical

picture [8,9] of their TI properties is not completely clear yet, but our results open the road to further experiments (on the dependence of the IEE on thickness, temperature, and gate voltage, not in the scope of this Letter) for a better understanding of this new TI. The final result, the much shorter relaxation time of the topological states at the α-Sn(001)|Ag interface in comparison with the relaxation time at TI free surfaces derived from time-resolved ARPES, is probably due to the electron exchange with the adjacent 3D metal layer, allowing us to anticipate much more efficient IEE at the interface of TIs with insulators.

We acknowledge Laura Bocher, Katia Marsch, and Odile Stéphan from the "Laboratoire de Physique des Solides" (Universite Paris-Sud) and David Troadec from the "Institut d'Electronique, de Microélectronique et de Nanotechnologie" (CNRS) for their help during the characterization of the samples. We thank I. Pheng for the preparation of the sample for SP-FMR.

*Present address: Institut Jean Lamour, UMR CNRS 7198—Université de Lorraine- B.P. 70239, F-54506 Vandoeuvre France.
juan-carlos.rojas-sanchez@univ-lorraine.fr
†nicolas.reyren@thalesgroup.com
‡albert.fert@thalesgroup.com

[1] *Handbook of Spin Transport, and Magnetism*, edited by I. Žutić and E. Y. Tsymbal (Chapman and Hall/CRC, 2011).
[2] S. O. Valenzuela and M. Tinkham, Direct electronic measurement of the spin Hall effect, Nature (London) **442**, 176 (2006).
[3] M. Cubukcu, O. Boulle, M. Drouard, K. Garello, C. O. Avci, I. M. Miron, J. Langer, B. Ocker, P. Gambardella, and G. Gaudin, Spin-orbit torque magnetization switching of a three-terminal perpendicular magnetic tunnel junction, Appl. Phys. Lett. **104**, 042406 (2014).
[4] C. R. Ast, J. Henk, A. Ernst, L. Moreschini, M. Falub, D. Pacilé, P. Bruno, K. Kern, and M. Grioni, Giant Spin Splitting through Surface Alloying, Phys. Rev. Lett. **98**, 186807 (2007).
[5] L. Fu, C. K. Kane, and E. J. Mele, Topological Insulators in Three Dimensions, Phys. Rev. Lett. **98**, 106803 (2007).
[6] M. Z. Hasan and C. L. Kane, Colloquium: Topological insulators, Rev. Mod. Phys. **82**, 3045 (2010).
[7] X.-L. Qi and S.-C. Zhang, Topological insulators and superconductors, Rev. Mod. Phys. **83**, 1057 (2011).
[8] L. Fu and C. L. Kane, Topological insulators with inversion symmetry, Phys. Rev. B **76**, 045302 (2007).
[9] Y. Xu, B. Yan, H. J. Zhang, J. Wang, G. Xu, P. Tang, W. Duan, and S. C. Zhang, Large-Gap Quantum Spin Hall Insulators in Tin Films, Phys. Rev. Lett. **111**, 136804 (2013).
[10] A. Barfuss *et al.*, Elemental Topological Insulator with Tunable Fermi Level: Strained α-Sn on InSb(001), Phys. Rev. Lett. **111**, 157205 (2013).
[11] Y. Ohtsubo, P. Le Fèvre, F. Bertran, and A. Taleb-Ibrahimi, Dirac Cone with Helical Spin Polarization in Ultrathin α-Sn(001) Films, Phys. Rev. Lett. **111**, 216401 (2013).
[12] V. M. Edelstein, Spin polarization of conduction electrons induced by electric current in 2D asymmetric electron systems, Solid State Commun. **73**, 233 (1990).
[13] P. Schwab, R. Raimondi, and G. Gorini, Spin-charge locking and tunneling into a helical metal, Eur. Phys. Lett. **93**, 67004 (2011).
[14] H. J. Zhang, S. Yamamoto, B. Gu, H. Li, M. Maekawa, Y. Fukaya, and A. Kawasuso, Charge-to-Spin Conversion and Spin Diffusion in Bi/Ag Bilayers Observed by Spin-Polarized Positron Beam, Phys. Rev. Lett. **114**, 166602 (2015).
[15] A. R. Mellnik *et al.*, Spin-transfer torque generated by a topological insulator, Nature (London) **511**, 449 (2014).
[16] C. H. Li, O. M. J. van 't Erve, J. T. Robinson, Y. Liu, L. Li, and B. T. Jonker, Electrical detection of charge-current-induced spin polarization due to spin-momentum locking in Bi2Se3, Nat. Nanotechnol. **9**, 218 (2014).
[17] J. Tang *et al.*, Electrical detection of spin-polarized surface states conduction in (Bi0.53Sb0.47)2Te3 topological insulator, Nano Lett. **14**, 5423 (2014).
[18] J.-C. Rojas-Sánchez, L. Vila, G. Desfonds, S. Gambarelli, J. P. Attané, J. M. De Teresa, C. Magén, and A. Fert, Spin-to-charge conversion using Rashba coupling at the interface between non-magnetic materials, Nat. Commun. **4**, 2944 (2013).
[19] K. Shen, G. Vignale, and R. Raimondi, Microscopic Theory of the Inverse Edelstein Effect, Phys. Rev. Lett. **112**, 096601 (2014).
[20] A. Nomura, T. Tashiro, H. Nakayama, and K. Ando, Temperature dependence of inverse Rashba-Edelstein effect at metallic interface, Appl. Phys. Lett. **106**, 212403 (2015).
[21] S. Sangiao, J. M. De Teresa, L. Morellon, I. Lucas, M. C. Martinez-Velarde, and M. Viret, Control of the spin to charge conversion using the inverse Rashba-Edelstein effect, Appl. Phys. Lett. **106**, 172403 (2015).
[22] W. Zhang, M. B. Jungfleisch, W. Jiang, J. E. Pearson, and A. Hoffmann, Spin pumping and inverse Rashba-Edelstein effect in NiFe/Ag/Bi and NiFe/Ag/Sb, J. Appl. Phys. **117**, 17C727 (2015).
[23] M. Isasa *et al.*, Origin of inverse Rashba-Edelstein effect detected at the Cu/Bi interface using lateral spin valves, Phys. Rev. B **93**, 014420 (2016).
[24] See Supplemental Material at http://link.aps.org/supplemental/10.1103/PhysRevLett.116.096602, which includes Refs. [25,26], for model calculations, ARPES data, and experimental details.
[25] D. Culcer, Transport in three-dimensional topological insulators: Theory and experiment, Physica E (Amsterdam) **44**, 860 (2012).
[26] H. Nakayama, K. Ando, K. Harii, T. Yoshino, R. Takahashi, Y. Kajiwara, K. Uchida, Y. Fujikawa, and E. Saitoh, Geometry dependence on inverse spin Hall effect induced by spin pumping in NiFe/Pt films, Phys. Rev. B **85**, 144408 (2012).
[27] Y. Shiomi, K. Nomura, Y. Kajiwara, K. Eto, M. Novak, K. Segawa, Y. Ando, and E. Saitoh, Spin-Electricity Conversion Induced by Spin Injection into Topological Insulators, Phys. Rev. Lett. **113**, 196601 (2014).

[28] P. Deorani, J. Son, K. Banerjee, N. Koirala, M. Brahlek, S. Oh, and H. Yang, Observation of inverse spin Hall effect in bismuth selenide, Phys. Rev. B **90**, 094403 (2014).

[29] L. Liu, A. Richardella, I. Garate, Y. Zhu, N. Samarth, and C. T. Chen, Spin-polarized tunneling study of spin-momentum locking in topological insulators, Phys. Rev. B **91**, 235437 (2015).

[30] O. Mosendz, V. Vlaminck, J. E. Pearson, F. Y. Fradin, G. E. W. Bauer, S. D. Bader, and A. Hoffmann, Detection and quantification of inverse spin Hall effect from spin pumping in permalloy/normal metal bilayers, Phys. Rev. B **82**, 214403 (2010).

[31] J. C. Rojas-Sánchez, N. Reyren, P. Laczkowski, W. Savero, J. P. Attane, C. Deranlot, M. Jamet, J. M. George, L. Vila, and H. Jaffres, Spin Pumping and Inverse Spin Hall Effect in Platinum: The Essential Role of Spin-Memory Loss at Metallic Interfaces, Phys. Rev. Lett. **112**, 106602 (2014).

[32] M. Jamali, J. S. Lee, J. S. Jeong, F. Mahfouzi, Y. Lv, Z. Zhao, B. K. Nikolić, K. A. Mkhoyan, N. Samarth, and J.-P. Wang, Giant spin pumping and inverse spin Hall effect in the presence of surface spin-orbit coupling of topological insulator BiSe, Nano Lett. **15**, 7126 (2015).

[33] J. Kim, P. Sheng, S. Takahashi, S. Mitani, and M. Hayashi, Spin Hall magnetoresistance in metallic bilayers, arXiv:1503.08903.

[34] C.-F. Pai, L. Liu, Y. Li, H. W. Tseng, D. C. Ralph, and R. A. Buhrman, Spin transfer torque devices utilizing the giant spin Hall effect of tungsten, Appl. Phys. Lett. **101**, 122404 (2012).

[35] M. Hajlaoui *et al.*, Tuning a Schottky barrier in a photoexcited topological insulator with transient Dirac cone electron-hole asymmetry, Nat. Commun. **5**, 3003 (2014).

[36] G. E. Bauer, E. Saitoh, and B. J. van Wees, Spin caloritronics, Nat. Mater. **11**, 391 (2012).